Electronic Supplementary Information (ESI):

Inkjet print microchannels based on liquid template

Yuzhen Guo [a,b], Lihong Li[a], Fengyu Li*[a], Haihua Zhou[a] and Yanlin Song*[a]

[a] *Beijing National Laboratory for Molecular Sciences (BNLMS), Key Lab of Green Printing, Institute of Chemistry, Chinese Academy of Sciences, Beijing 100190, China. E-mail: ylsong@iccas.ac.cn; forrest@iccas.ac.cn*

[b]*Graduate University of the Chinese Academy of Sciences, Beijing 100049, P. R. China*

S 1.Preparation of printable ink

To control the morphology stability of the liquid template, undecanol is used as the main component of the ink due to its temperature-controllable viscosity. However, the undecanol is unprintable at room temperature (22℃) due to its high viscosity (15.2 mPa·S). To make the undecanol printable at room temperature, ethyl lactate is added into the ink to decrease the viscosity of undecanol (9.8 mPa·S) in the mass fraction of 1/4. The rheology properties of undecanol and the ink containing undecanol and ethyl lactate are shown in **Fig. S1**. The viscosity of undecanol is sensitive to temperature in the range of 20 ℃ to 10 ℃. And the viscosity of the ink containing undecanol and ethyl lactate is sensitive to temperature in the range of 20 ℃ to about 3 ℃.

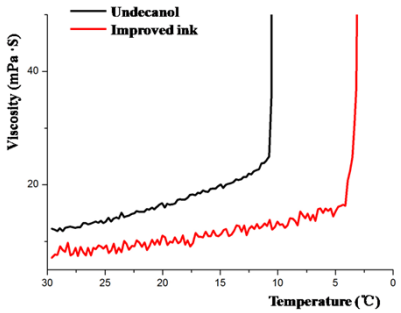

Fig. S1 Rheology properties of undecanol and ink containing ethyl lactate.

Table S1 Density of the ink and PDMS prepolymer mixture

	Test time	Weight/g	Volume/ml	Density/g • ml^{-1}	Average density/g • ml^{-1}
Ink	1#	6.023	7	0.860	0.86
	2#	6.911	8	0.864	
	3#	8.628	10	0.863	
Prepolymer mixture	1#	5.189	5.1	1.017	1.04
	2#	7.614	7.2	1.058	
	3#	5.710	5.5	1.038	

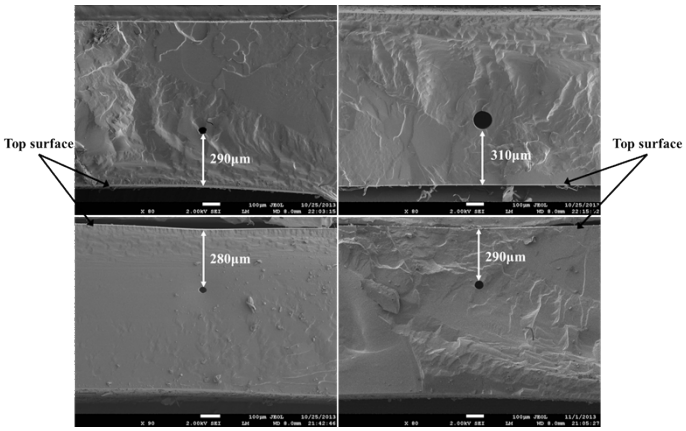

Fig.S2 The depths of channels in PDMS matrix.

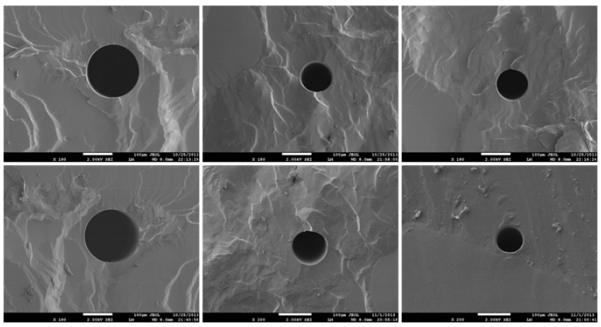

Fig. S3 More cross sectional SEM images of microchannels.

S2. Curvature analysis of the branched microchannel

In the case of branched liquid template, the sharp angle between adjacent branches forms a small curvature radius (R_{out} in **Fig. S4**). While the curved liquid surface forms a curvature radius (R_{in} in **Fig. S4**). As shown in **Equation. Group S1**, the Laplace pressure P_{out} caused by the R_{out} is greater than the P_{in} caused by the R_{in}, which drives the mass transfer to the joint. The mass transfer increases the R_{out} and decrease the P_{out}. When the R_{out} is equal to R_{in}, the mass transfer stop and the sharp angle transforms to fillet angle.

$$P_{out} = 2\gamma/R_{out}, \; P_{in} = 2\gamma/R_{in}$$

$$\text{And} \quad R_{out} < R_{in} \qquad \textbf{(Equation. Group S1)}$$

$$\text{So} \quad P_{out} > P_{in}$$

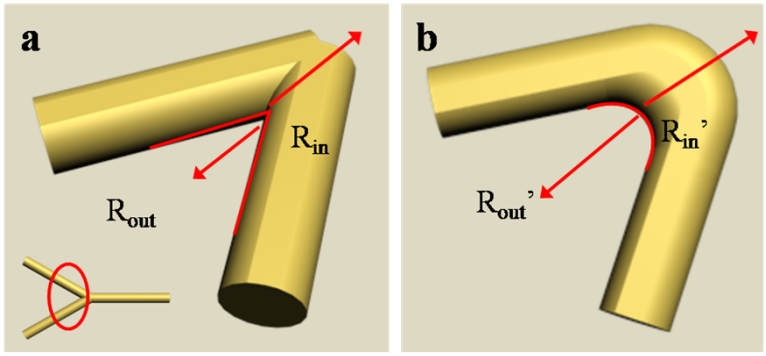

Fig. S4 Scheme of the curvature analysis for mass transfer

S3. Curvature analysis of the junction between two channels with very different diameters

In the case of a junction between two channels with different diameters, the mass transfer driven by curvature difference should be taken into consideration. **Fig S5 (a)** schemes a newly prototyped junction, which has four curvature radius. R_1 and R_2 ($R_1 > R_2$) represent the curvature radius of the two channels, respectively, while R_{S1} and R_{S2} are the curvature radius of the sharp corners at the junction. $R_{S1}$and R_{S2} are far smaller than R_1 and R_2. The corresponding Laplace pressure equations are as follows:

$$P_1 = 2\gamma/R_1,\ P_2 = 2\gamma/R_2$$

$$P_{S1} = 2\gamma/R_{S1},\ P_{S2} = 2\gamma/R_{S2}$$

$$\text{And} \qquad R_{S1}, R_{S2} < R_1, R_2$$

$$\text{So} \qquad P_{S1}, P_{S2} > P_1, P_2$$

According to the equations above, the Laplace pressures P_1 and P_2 caused by R_1 and R_2 are larger than the P_{S1} and P_{S2} caused by the R_{S1} and R_{S2}. The Laplace pressure difference would result in mass transfer to decrease curvature difference. The directions of the mass transfer are supposed to be along with the radial direction of $R_{S1}$and R_{S2}, which point inside and outside of the template, respectively.

The mass transfer would lead to two phenomenons. Firstly, a curvature gradient between the two channels forms and the junction becomes smooth (Place I in **Fig. S 5 (b)**). Secondly, the mass transfer also results in the change of the channel radius. The region of the channel near the junction becomes thinner (taking Place II in **Fig. S5 (b)** for example) than the rest of the same channel ($R_2' < R_2''$).

Due to the high viscosity of the ink in the paper, the mass transfer driven by the curvature difference would become slower and ignorable as the pressure gradient reaches a certain value. Then, the junction becomes stable. To verify the analysis above, a junction between a channel with a diameter of about 200μm and the other with about 600 μm is fabricated, as shown in **Fig. S5 (c)** (Note: a serial of optical images are integrated together).

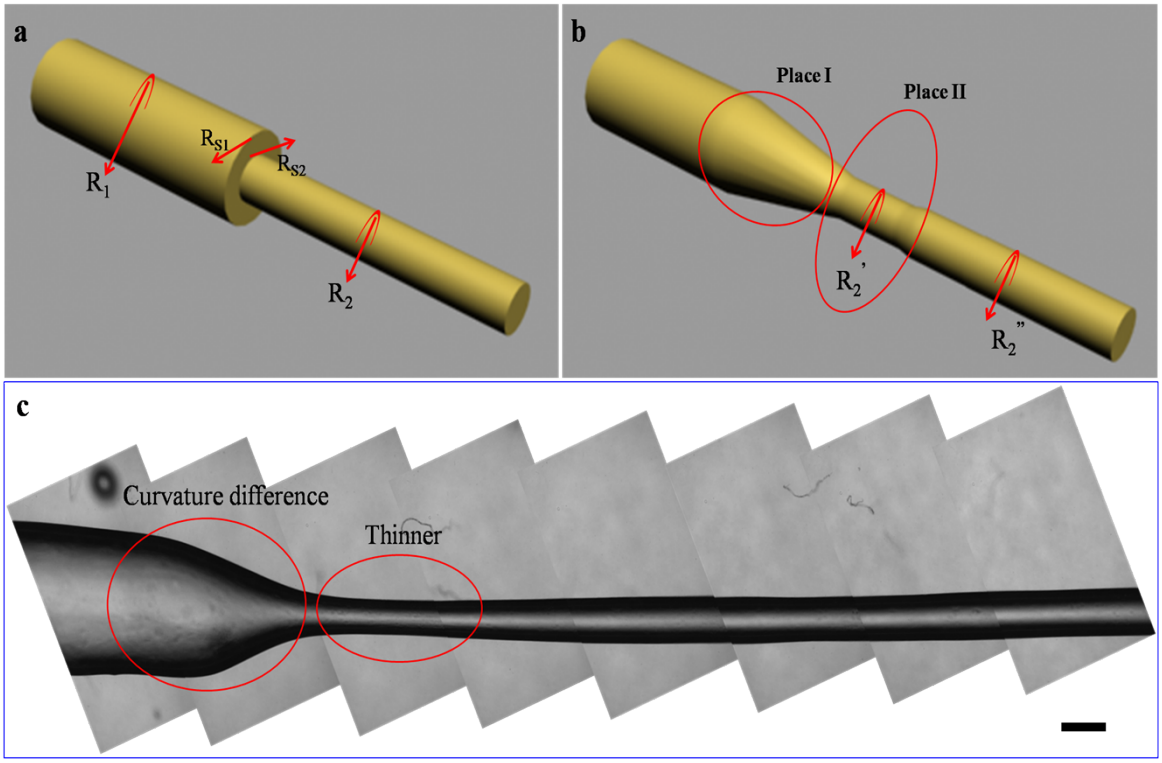

Fig. S 5 (a) Sketch of the newly prototyped junction between two channels with different diameters; **(b)** Sketch of the junction after mass transfer driven by curvature difference; **(c)** The junction between channel with diameter of about 200 μm and channel with diameter of about 600 μm (scale bar=200 μm).

S4. Fabrication resolution of microchannels

In addition to the microchannels with the diameters ranging from 200 to 900 μm (as shown in **Figure 2(b) (d)**), the microchannels with the diameter smaller than 100 μm have also been fabricated. **Fig. S6** exhibits the channels with the diameter of about 50 and 25μm. So far, the highest resolution of this approach is about 25 μm (**Fig. S6 (a)**).

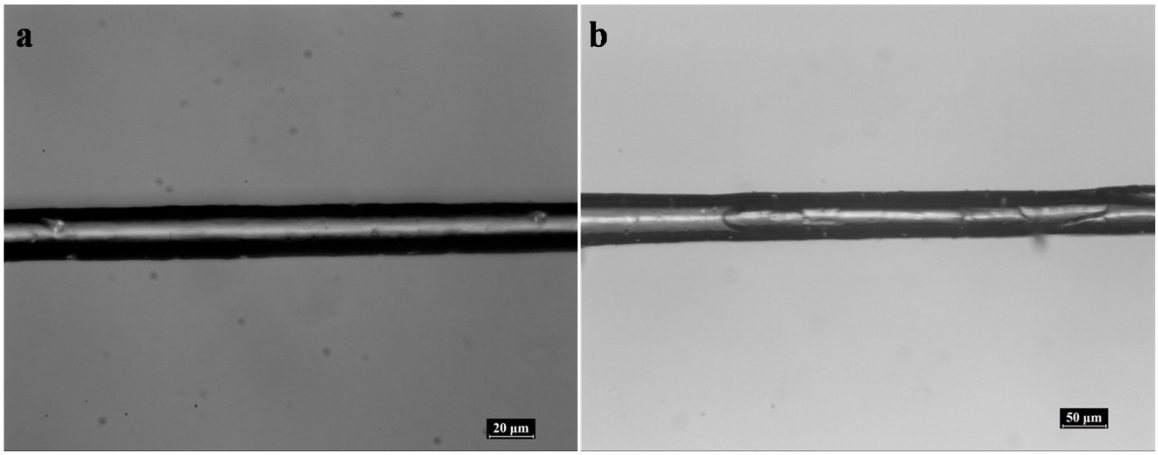

Fig. S6 Microchannels with the diameters of about 25μm (a) and 50 μm (b).

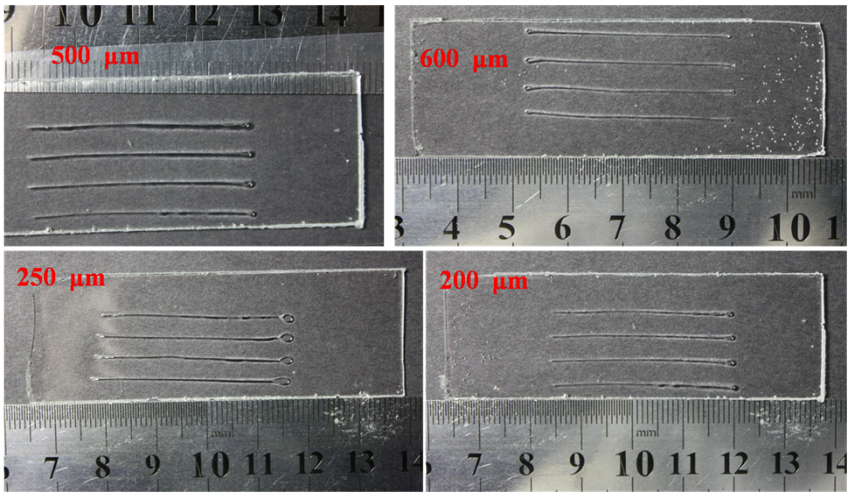

Fig. S7 Microchannels with the diameters of about 200μm ~600 μm.

Eq. S1 Chemical reaction of the polymerization and modification during the formation of micorchannel

$$R_3SiH+CH=CH\text{-}R' \xrightarrow{\text{Catalyst}} R_3Si\text{-}CH\text{-}CH\text{-}R' \quad (1)$$

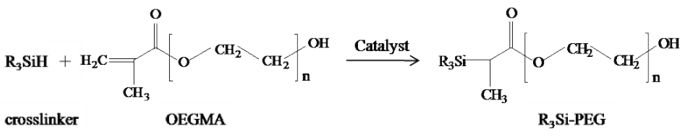

(2)

S5. Confirmation of PEG on the internal surface of modified microchannels

The high resolution X-ray photoelectron spectra (XPS) of C 1s peaks were recorded to confirm the existence of PEG groups on the internal surface of PEG modified micorchannels. **Fig. S8** shows the main C 1s peak (C-H) of the unmodified PDMS microchannels at the binding energy of 285 eV. While an extra peak in the C 1s region at 286.7 eV attributed to carbons bond to PEG oxygen atoms (C-O), about 1.7 eV higher than the main C 1s peak (C-H) at 285 eV appears on the internal surface of PEG modified PDMS microchannel. Furthermore, elemental quantitative analysis by XPS is carried out and shown in **Table S2**. The result reveals an increase in the amount of C atoms and O atoms, while a decrease in the amount of Si atoms in the PEG modified PDMS channel surface.

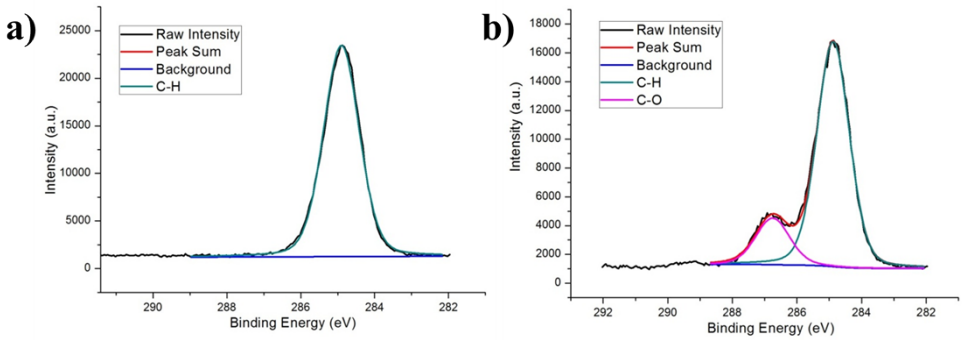

Fig. S8 High resolution XPS spectra of C 1s peaks of the internal surface of the unmodified PDMS microchannel **(a)** and the PEG modified microchannel **(b)**.

Table S2 General Ratio of the elements of PDMS and PEG modified PDMS microchannel internal surface

	C		O	Si
Sample	C-H	C-O		
unmodified	—	45.3	28.2	26.5
PEG modified	40.3	8.7	29.1	21.9

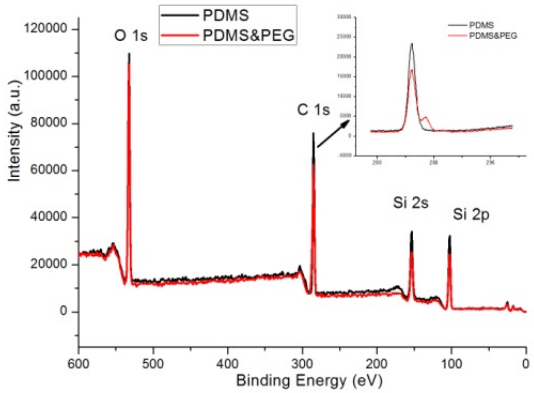

Fig. S9 XPS spectra of PDMS (in black) and PEG modified (in red) microchannel internal surface

S6. Different capillary rise between unmodified microchannel and PEG modified microchannel

To investigate the wetting properties of the PDMS microchannels and the PEG modified microchannels, capillary rise tests were carried out. Microchannel was perpendicularly placed with one end immersed into water. OCA20 machine was used to observe the height of capillary rise of water in microchannels. **Fig. S10** shows the images of the capillary rise of water in PDMS microchannel and PEG modified microchannel.Due to the hydrophobicity of the PDMS, there is no capillary water rise in the unmodified PDMS microchannel. While in the PEG modified microchannel, a capillary water rise is observed obviously due to the hydrophilic hydroxyl group.

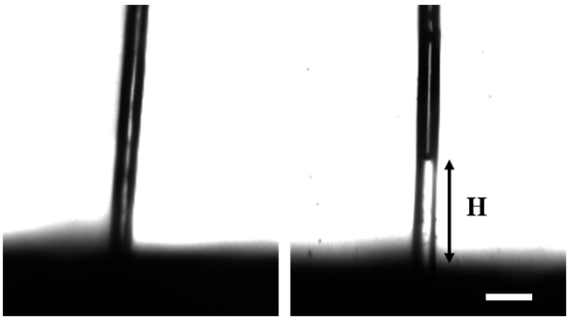

Fig. S10 The images of the capillary rise of water in unmodified microchannel (left) and PEG modified microchannel (right) (scale bar=1000 μm).